Analysis of Permeability, the Effects on Flow Properties, and Applications of Porous Fibrous Metal Aluminums

Sponsored by Shibaura Institute of Technology

Author:

Talia Brooks

Advisor:
Adam Powell

October 10th 2019

Abstract

Because of their unique physical structures and advanced heat transfer and flow properties, porous metals are sought after for a wide range of applications. This study focuses on finding potential applications of four differing samples of a new porous fibrous metal made by Mitsubishi Materials based on the analysis of the effects of permeability on the flow and heat transfer properties. Two different experiments were used to measure the average flow velocity and pressure drop in order to find permeability. Computer simulations were used to further identify flow behaviors based on the average flow velocity and pressure drop. It was found that in both the experimental and simulation methods, all samples showed high permeability value estimations. Both methods showed that as porosity and wire diameter increases, permeability increases. Generally, higher permeability values were found to be desirable for applications with fluid or air flow. In finding and understanding the properties of the samples used in this study, and how these properties affect their performance in a wide range of applications, they can used to their full potential.

Introduction

In recent years, porous metals have become increasingly interesting for their multiple functionality in fluid dynamics, heat transfer enhancement, and electrical conduction. These phenomena are useful in a multitude of different processes due to characteristics like high surface area to volume ratio, generally low weight, high electrical conductivity, and beneficial pore structure. Heat regenerators [1], filtration devices [2, 3], noise pollution prevention, fireproofing [4], supercapacitors, and batteries [5] are just a few of many of the versatile applications of porous metals that occur in our daily lives.

Despite the multitude of studies on porous metals such as metal foams, sheets, and porous fibrous cylinders and rectangular prisms, new porous metals' properties must be individually tested. The complex and random physical structure of some porous metals make it difficult to universally understand the fluid flow characteristics of porous metals. This study explores the fluid flow characteristics of a new type of material manufactured by Mitsubishi Materials in order to best utilize the material in selected applications. More specifically, this study focuses on measuring the permeability of porous metals to understand the fluid flow features of this new type of porous fibrous metal.

In this study, experiments were conducted to measure the permeability of a porous fibrous medium by measuring the flow of a viscous fluid through mass and pressure. Computer simulations of fluid flow were also used to estimate permeability in similar porous media, for comparison with experiments. From these measurements and estimates of permeability, relationships between permeability and thermal behaviors establish grounds for estimates of heat transfer coefficients, and thus, appropriate applications for the new medium created by Mitsubishi Materials were determined.

Background

Nomenclature

Term	Symbol	Definition
Reynolds Number	*Re*	dimensionless parameter for the measurement of viscous fluid flow
Nusselt Number	Nu	dimensionless heat transfer coefficient
Prandtl Number	Pr	measure of relative thickness of the velocity and thermal boundary layer
Darcy Flow	Q	a type of flow where the pressure gradient and velocity are directly proportional
Permeability	K	a measure of the capacity and ease of flow of liquid through a medium
Porosity	ϕ	geometrical property that measures the fluid storage capacity of the porous structure
Computational Fluid Dynamics	CFD	the use of computer simulations to estimate properties of fluid flow in a material

Source: [6]

Permeability and Previous Studies

Many studies have been conducted on porous media similar to those used in this study. It is important to understand how the physical structure of porous metals in turn affect fluid flow and heat transfer characteristics. J. M. Baloyo explores different processes and resulting thermo-fluid characteristics for various porous metals. This review in turn analyzes recent applications of porous metals in thermal management based on the above parameters. It was found that the physical structure present as a result of the manufacturing process strongly influence characteristics like fluid flow, and in turn, the heat transfer properties of the metal [7]. The study noted that for low Reynolds number, the flow was laminar, or that the velocity was directly proportional to the pressure gradient. Darcy flow and low Reynolds number are shown to be important factors in the optimal settings for fluid flow when testing permeability in porous metals. Baloyo's paper also highlights the lack of research on metals with

non-uniform pore structures, the type of structure of which we are concerned with in this paper.

3D modeling is a useful way to measure flow rates and permeability through the ease of changing parameters such as the liquid used and pressure to test a wide range of situations for different porous metals. The study by Huang et al analyzes flow permeability in porous metal fiber sintered sheets (PMFSS) through X-ray tomography and the lattice Boltzmann method [8]. Huang et al's study uses porous metal fiber sheets with average diameter of 100μm and porosities of 75%, 80%, and 90% porosity. Permeability was obtained in steady state conditions. Similar to parts of this study, the Huang et al report uses 3D modeling and simulations to determine permeability. The study determined that simulated permeability increases in precision with size and voxel (3D volume unit) resolution, reliable permeability measurements are possible through use of small or low resolution representative volume element (RVE, the smallest approximate cross-sectional volume used to estimate the behaviors of the whole sample), and verified a direct connection between permeability and square pore diameters as well as microstructure and permeability (through the quantification equation). 3D modeling can, however, present difficulties when trying to test non-uniform pore structures.

A study by Jain et al uses CFD software compare heat transfer from both porous-permeable spheres and solid spheres as a result of fluid flow based on Re, Pr, Nu, and permeability ratio. It was found that at low Re and Pr, the Nu for a permeable sphere was higher than that of an impermeable sphere. At high Re, the Nu for a permeable sphere was significantly higher than that of an impermeable sphere, regardless of Pr [9]. The study also found a linear relationship between heat transfer rates and permeability. This relationship suggests that a high Nu could result in high permeability.

The study by Tasaka et al uses pressure drop as a parameter for measuring convective heat transfer in porous metals by quantifying the capillary forces and measuring the osmotic power of the porous samples. The study uses porous fibrous metals also manufactured by Mitsubishi materials. The study found that heat transport as a result of convective heat transfer was higher in sample of high porosity when compared to that of lower porosity, shown by the high Nusselt numbers of highly porous materials [10]. Pressure drop has been found to be dependent on permeability per area, and sequentially, on heat dispersion. This suggests that high permeability would result in high heat dispersion during heat transfer processes. The authors thus concluded there was a potential high correlation between permeability and heat transfer properties during Darcy flows and suggested further testing on permeability for the Mitsubishi Materials samples. The research discussed in this paper is a continuation of the findings in the Tasaka et al study, and a collaboration with the group.

Comprehensively, it is evident from many similar studies on porous metals that properties of physical structure of a test sample directly correlate with fluid flow behaviors. Fluid flow measurements are an accurate way to understand the permeability of the medium. In turn, permeability can be used to estimate a number heat transfer characteristics. Through understanding the relationship between porosity, permeability, and heat transfer abilities in porous metals, it is possible to then best apply different types of porous metals to a wide range of operations. Understanding the permeability of a porous metal is very meaningful for understand fluid flow and heat transfer behaviors as a whole.

Methodology

Both experiments and computer simulations were used in this study to estimate the flow properties and understand the permeability of porous fibrous metals.

Experimental Sample Characteristics

In experimental computations for this study, four different cylindrical porous media of varying fiber diameter and porosities were used. Fig. 1 shows the shared characteristics of each of the four samples used in experimentation. Wire diameters of either 200 μm or 500 μm, and porosities of either 75% or 85% were parameters set in samples of this study. The specific porous media used were, 200-75, 200-85, 500-75, 500-85, read as 'fiber diameter value-porosity value.'

Material	Aluminum
Process	Laminated, sintered
Length (mm)	10
Diameter (mm)	10

Fig. 1 - Table of shared characteristics of experimental samples

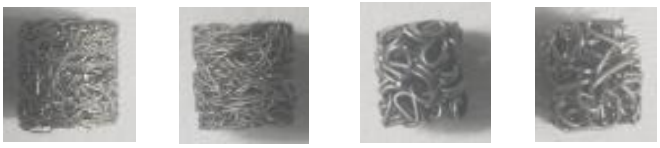

a – 200-75 b – 200-85 c – 500-75 d – 500-85

Fig. 2 – CAD models, a: 200-75, b: 200-85, c: 500-75, d: 500-85

Experimental Methods

Both experimental apparatus were designed to characterize the fluid flow of viscous oils through the porous samples at timed intervals. Measurements of mass and pressure were taken during the experiment to then calculate the pressure gradient, average flow velocity, and finally permeability based on the aforementioned values.

The first experimental apparatus is show in Fig. 3. In experimental method one, each trial began by applying pressure to the system that began the flow of silicone oil through the testing apparatus. Once the pressure of the system and the flow of the liquid were both stable, the beaker below the tap was replaced to collect the flowing silicone oil. After 300 seconds, the beakers were once again switched, and the pressure at the time of switching was noted. The mass of the experimental beaker was then measured and

this process repeated until three total mass and pressure readings were recorded. Before each new set of trials, a weight is taped to the syringe plunger, and the experiment is repeated. The experiment ended after four full trials.

Experimental method two consisted of a similar experimental set up and process, but used a more viscous silicone oil. The experimental set up is shown in Fig. 3. The second experimental method began by adding weights to the tray to begin the flow of oil. Once the pressure of the system no longer increased, the beaker under the tap was interchanged to collect the silicone oil flowing through the system. Since this oil is highly viscous, and thus flows more easily, collections lasted 120 seconds before the beakers were once again changed. The beginning pressure, ending pressure, and mass were recorded for each collection. After 360 seconds, a new full trial begins. A tray was fixed to the head of the syringe in order to add weights before beginning each set of trials. The experiment ends after nine full trials.

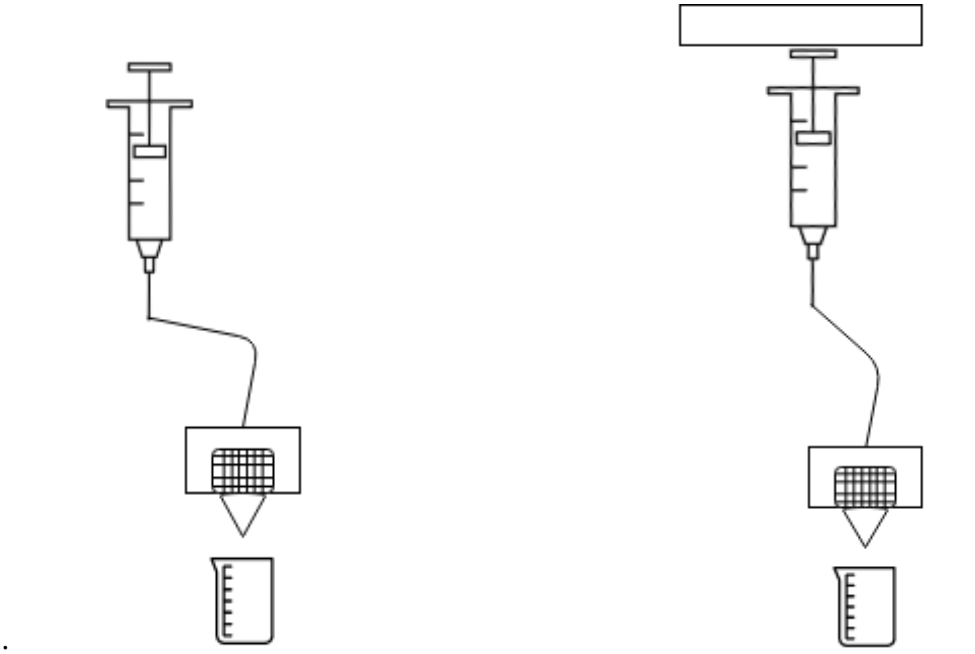

a – Experimental set up one

b – Experimental set up two

Fig. 3 - Experimental Set Ups: Fig. a - experimental set up one, Fig. b, experimental set up two

A detailed protocol of each experimental method can be found below:

Experimental Method One

1. Weigh the experimental beaker, record initial mass
2. Place collection beaker under outlet spout to catch flowing oil
3. Open outlet spout to allow flow of silicone oil, turn on pressure gauge
4. Secure one weight (approx. 109g) to the neck of the plunger and push down slightly to begin fluid flow
5. Allow the pressure to increase until reaching a stable value
6. Once the pressure is consistently stable and no longer rising, switch the collection beaker with the experimental beaker, and record pressure at time of beaker switch
7. Begin timed oil collection for five minutes
8. Once five minutes has passed, replace the experimental beaker with the collection beaker under the outlet spout
9. Weigh the experimental beaker, record the mass
10. Push down slightly on the plunger neck
11. Repeat steps 5-9 twice to obtain data for one trial
12. To begin a new trial, repeat steps 4-11
13. Conduct experimentation for four total trials for each sample

Experimental Method Two

1. Weigh the experimental beaker, record initial mass
2. Place collection beaker under outlet spout to catch flowing oil
3. Open outlet spout to allow flow of silicone oil, turn on pressure gauge
4. Place three weights (approx. 327g) into the tray secured to the top of the syringe plunger
5. Adjust the plunger so it is parallel with the body of the syringe
6. Allow the pressure to increase until reaching a stable value
7. Once the pressure is consistently stable and no longer rising, switch the collection beaker with the experimental beaker, and record pressure at time of beaker switch
8. Begin timed oil collection for two minutes
9. Once two minutes has passed, replace the experimental beaker with the collection beaker under the outlet spout, record the pressure at time of beaker switch
10. Weigh the experimental beaker, record the mass
11. Repeat steps 5-9 twice to obtain data for one trial
12. To begin a new trial, add a weight (approx. 109g) to the tray
13. Repeat steps 4-12
14. Conduct experimentation for nine total trials for each sample

Experimental method two was created to further improve results gained from experimental method one. Adding a tray to the plunger allowed for weights to be more easily added to the system. The elimination of pushing the plunger down and instead allowing only the weights to stabilize the pressure removed much of the fluctuation and discrepancies in the pressure readings. Particularly in changing the liquid used from a low viscosity to a higher viscosity liquid, the average flow velocity can be more accurately measured.

CFD Sample and Simulation Characteristics

In this study, CFD modeling was used to estimate the flow properties of four different samples using pressure drop. The "PHOENICS" CFD program used is able to simulate a wide range of thermal fluid applications [11].

The 3-D CAD models used in simulations were simplified lattice structures. The cubic geometry was

created by small circular extrudes on the x, y, and z axes that act to create fibers. The diameters of the wires were either 200µm or 500 µm, and had porosities of either 75% or 85%, just like the experimental samples as shown in Fig. 4. The length of the models was decided based on the aforementioned properties. Although the physical structures of the experimental apparatus and CAD model used in simulations are different, they share the same properties such as material, porosity, fiber diameter, and surface area.

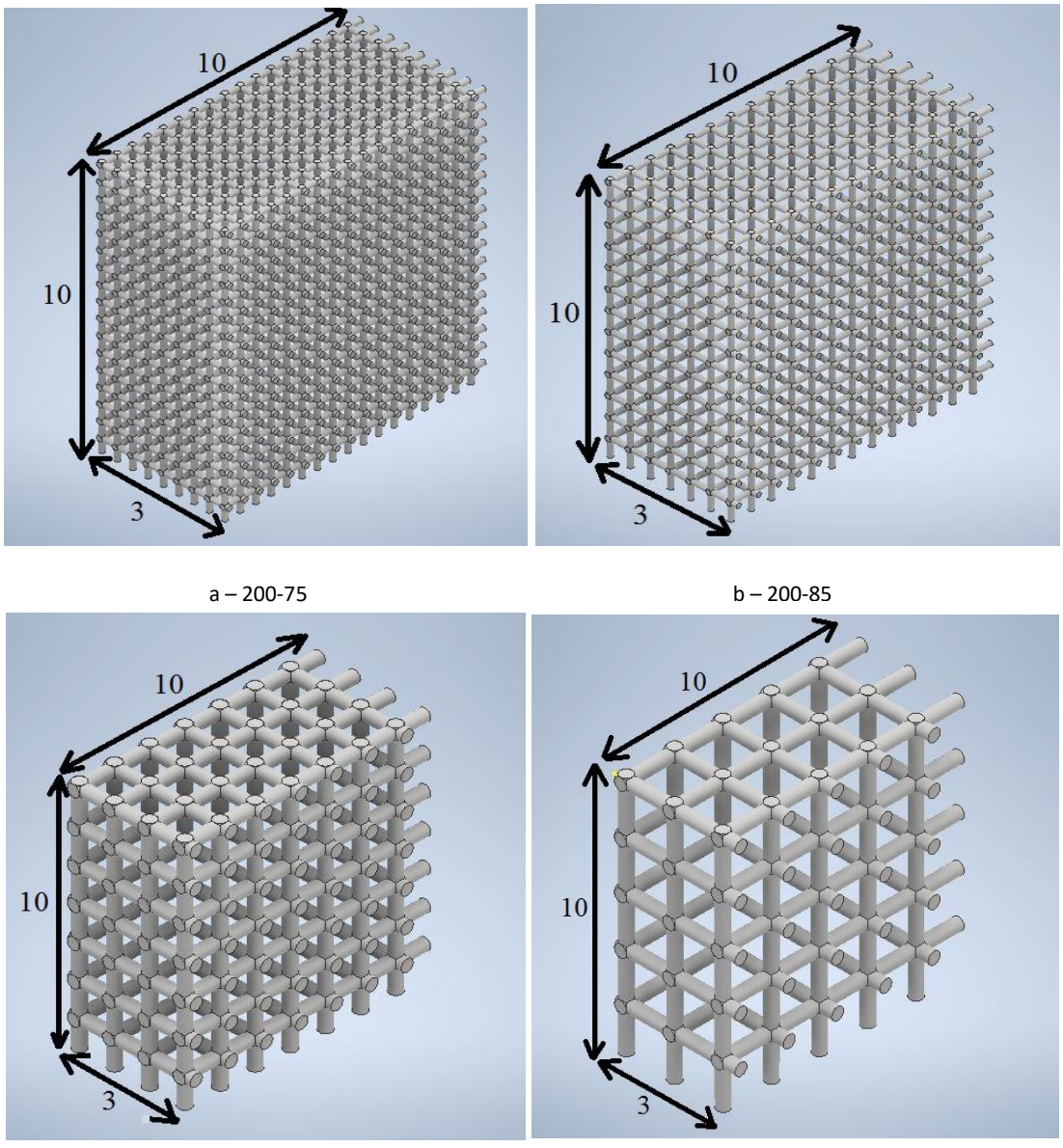

Fig. 4 – CAD models, a: 200-75, b: 200-85, c: 500-75, d: 500-85

The simulation set up consisted of a rectangular chamber, an inlet and outlet at each end, blockages lining the top and bottom of the chamber, and flow path walls along the front and rear faces. On the bottom face, there are three blockages, of which the CAD model was placed in the center blockage as shown in Fig. 5.

The Cartesian grid function was used to generate the numerical grid, and used a total of 889, 280 cells total in the grid. In the domain of each porous medium used in the simulations, there are 500 cells. Fig. 6 details the distribution of cells in the system overall.

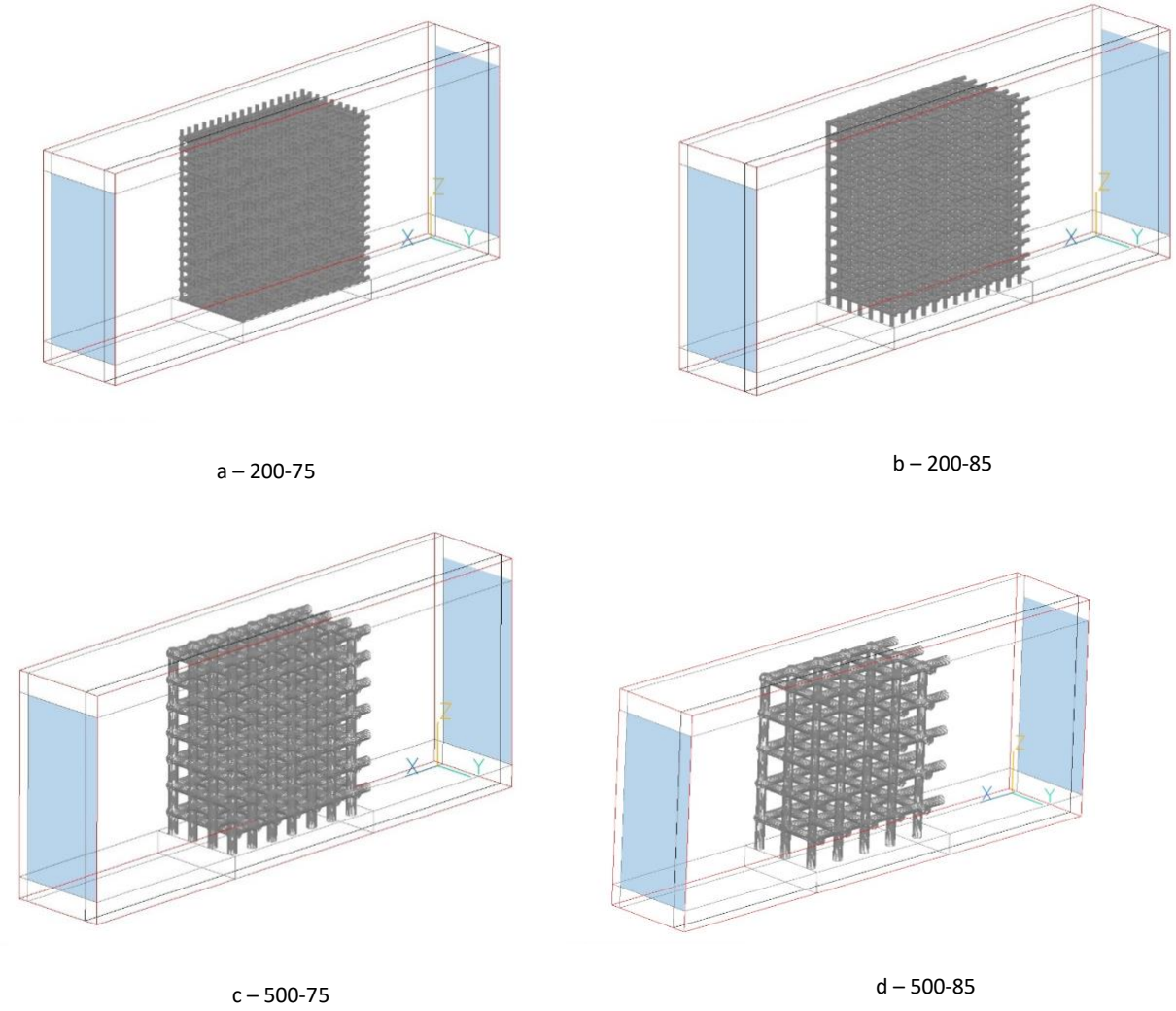

a – 200-75

b – 200-85

c – 500-75

d – 500-85

Fig. 5 – Numerical models, a: 200-75, b: 200-85, c: 500-75, d: 500-85

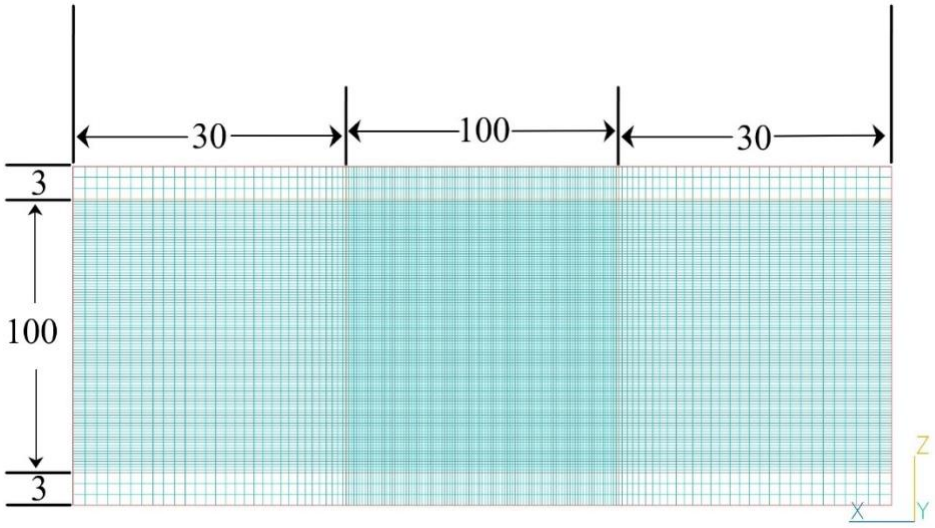

a – x-z coordinate plane

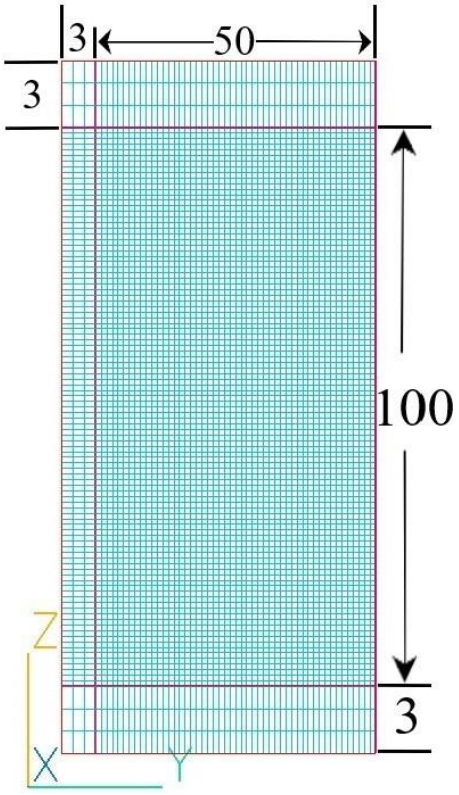

b – y-z coordinate plane

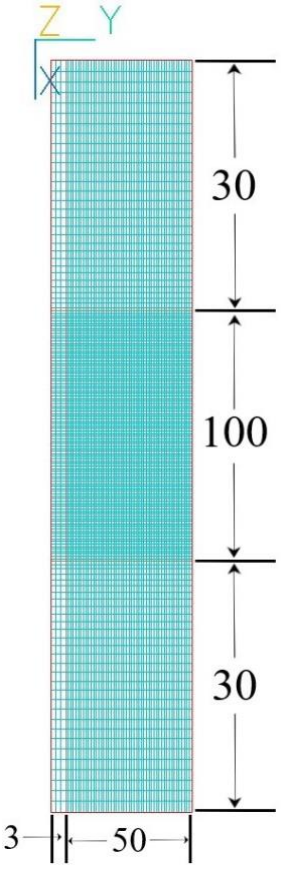

c – x-y coordinate plane

Fig. 6 - Grid cell counts in numerical models, a: x-z coordinate plane, b: y-z coordinate plane, c: x-y coordinate plane

Parameters for each simulation were set based on calculations of average pressure gradient values obtained from each set of experiments for each porous medium. Fig. 7 shows the average pressure gradient values for each porous medium model analyzed.

	Average Pressure Gradient Values (Pa/m)			
200-75	1.4×10^6	1.5×10^6	2.45×10^6	2.825×10^6
200-85	7×10^5	8.5×10^5	1.075×10^6	1.45×10^6
500-75	5.25×10^5	6.25×10^5	7.375×10^5	9×10^5
500-85	2×10^5	2.5×10^5	2.75×10^5	3.725×10^5

Fig. 7 - Average pressure gradient values

Results and Discussion

Experimental Method One Results

During experimentation, the mass and pressure values were recorded every 300 seconds. From these values, a number of properties were calculated based on the relationships from Eqs. 1

$$\frac{\Delta P}{L} = \frac{\mu}{K} V \tag{1}$$

The pressure values were first converted into kPa and then the pressure gradient (Δ) was calculated using Eqs. 2

$$\Delta P = \frac{P \cdot 10^3}{L} \tag{2}$$

where P was pressure (kPa) and L is the length of the porous medium (m).

Next, Eqs. 3 was used to calculate the mass flow rate (ṁ) for each case,

$$\dot{m} = \frac{\Delta M}{\Delta T} \tag{3}$$

where ΔM is the change in mass reading per case in each trial, and ΔT is the change in temperature from case to case in each trial.

Following these calculations, the average flow velocity ($\dot{v}_{avg}$) was found for each case as shown by Eqs. 4

$$\dot{v}_{avg} = \frac{\dot{m} \cdot 10^{-3}/\rho}{25 \cdot \pi \cdot 10^{-6}} \tag{4}$$

where ṁ is the mass flow rate and ρ is the density of the working liquid.

The averages of the average flow velocity values and the pressure gradient values for each trial were determined. These average values were next plotted and slope was calculated. Finally, the viscosity of the working liquid was divided by the slope generated to find the permeability for the sample as shown in Fig. 8.

	Viscosity(Pa·s)	Slope	Permeability (m²)
200-75	97.4	$3.37705 \cdot 10^{11}$	$2.88417 \cdot 10^{-10}$
200-85		$1.06344 \cdot 10^{11}$	$9.15899 \cdot 10^{-10}$
500-75		$6.26873 \cdot 10^{10}$	$1.55374 \cdot 10^{-9}$
500-85		$1.79447 \cdot 10^{10}$	$5.42778 \cdot 10^{-9}$

Fig. 8 - Table of values used to calculate permeability

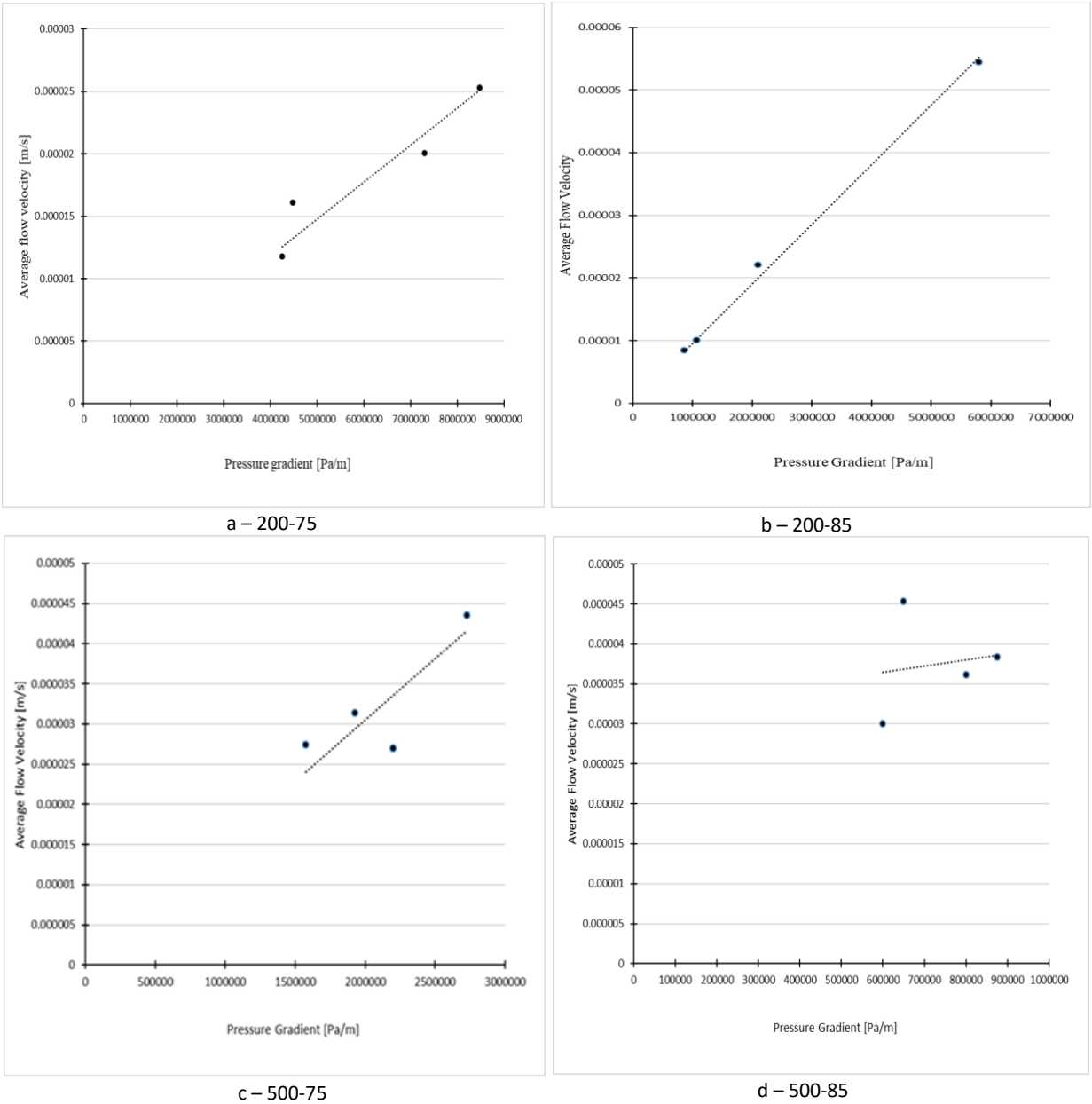

a – 200-75

b – 200-85

c – 500-75

d – 500-85

Fig. 9 - Relationship between the average flow velocity and pressure gradient, a: 200-75, b: 200-85, c: 500-75, d: 500-85

Experimental Method Two Results

Fig. 9 - Relationship between the average flow velocity and pressure gradient, a: 200-75, b: 200-85, c: 500-75, d: 500-85

During experimentation, the mass was recorded every 120 seconds. Pressure was recorded at the beginning and end of every 120 second sample collection based on the relationships presented in Eqs. 1.

The pressure values were first converted into kPa and then the pressure gradient (Δ) was calculated using Eqs. 5

$$\Delta P = \frac{P_{avg} \cdot 10^3}{L} \tag{5}$$

where P_{avg} was the average of the beginning and ending pressures every 120 second case (kPa) and L is the length of the porous medium (m).

Next, Eqs. 3 was used to calculate the mass flow rate ($\dot{m}$) for each case and the average flow velocity ($\dot{v}_{avg}$) was found for each case as shown by Eqs. 4 as mentioned in experimental method one's results. The averages of the average flow velocity values and the pressure gradient values for each of the nine trials were determined. These average values were next plotted and slope was calculated and the viscosity of the working liquid was divided by the slope generated to find the permeability for the sample as shown in Fig. 10, similar to the process used in experimental method one's results.

	Viscosity(Pa·s)	Slope	Permeability (m^2)
200-75	9.74	$9.70032 \cdot 10^9$	$8.22035 \cdot 10^{-9}$
200-85		$4.00581 \cdot 10^9$	$1.99061 \cdot 10^{-8}$
500-75		$2.31325 \cdot 10^9$	$3.44717 \cdot 10^{-8}$
500-85		$4.00581 \cdot 10^9$	$8.69059 \cdot 10^{-7}$

Fig. 10 - Table of values used to calculate permeability

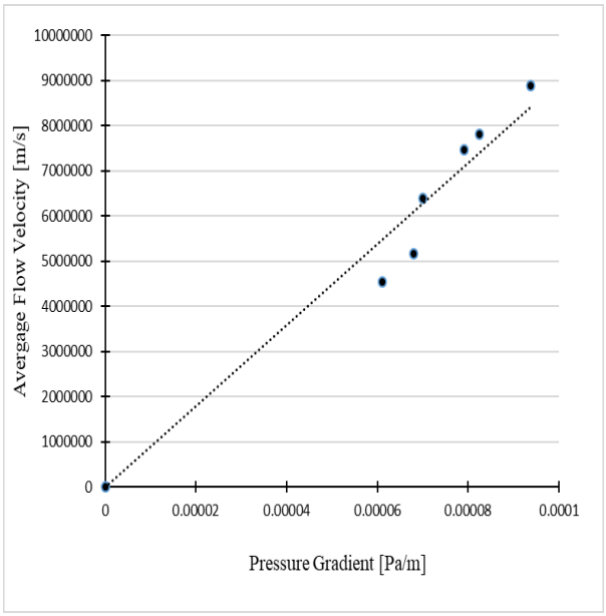

a – 200-75

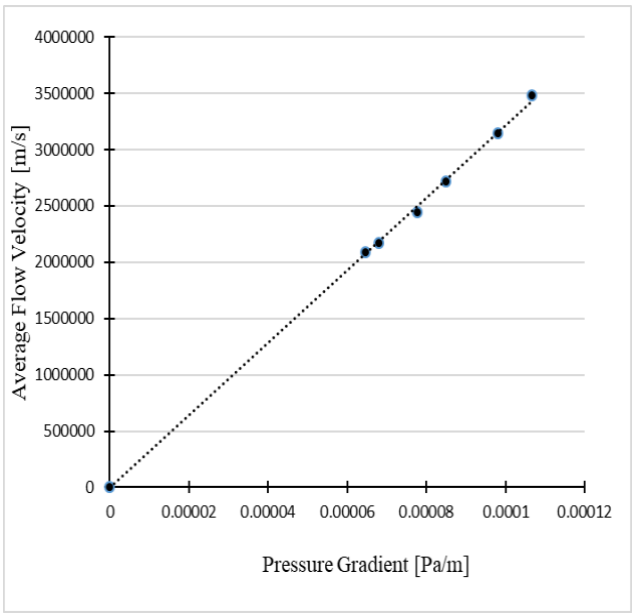

b – 200-85

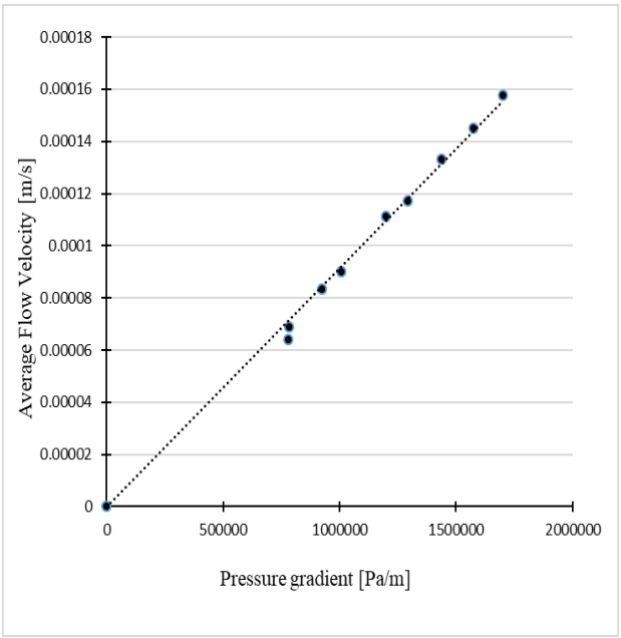

c – 500-75

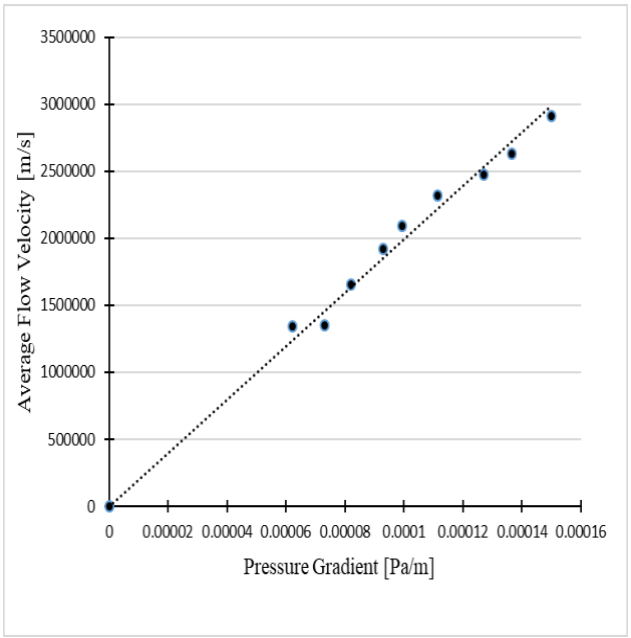

d – 500-85

Fig. 11 - Relationship between the average flow velocity and pressure gradient, a: 200-75, b: 200-85, c: 500-75, d: 500-85

Properties from experimental method one were used to estimate properties for simulations. Experimental method one's results showed more fluctuation and variation in permeability values, while experimental method two's results showed more of a stable, uniform change between the four samples. This difference between the two methods can be attributed to the change in viscosity between the working liquids used.

The second method used a more viscous liquid, which allowed the flow to be more easily and accurately measured, in turn allowing for more accurate permeability measurements.

Both methods show a clear link of the influence of fiber diameter and porosity on the permeability. The more porous metals were more permeable compared to the samples of the same fiber diameter.

The porous media with 85% porosity were shown to have more uniform relationships between average flow velocity and pressure gradient than those of 75% porosity. The metals with thicker fiber diameters were also more permeable than those of the thinner fiber diameter. Both methods showed the high permeability of each of the samples overall.

CFD Results

For each simulation, 1,000 iterations were set and the average flow velocity was calculated per 100 iterations. There values were again averaged to obtain a single average flow velocity per pressure gradient values. The average flow velocity and pressure gradient value were then graphed and using the slope of the line and viscosity of the working liquid (water), the permeability is calculated. Fig. 12 shows the graphs of average flow velocity versus pressure gradient of each sample. For each graph, a linear relationship can be seen between the average flow velocity and the pressure gradient.

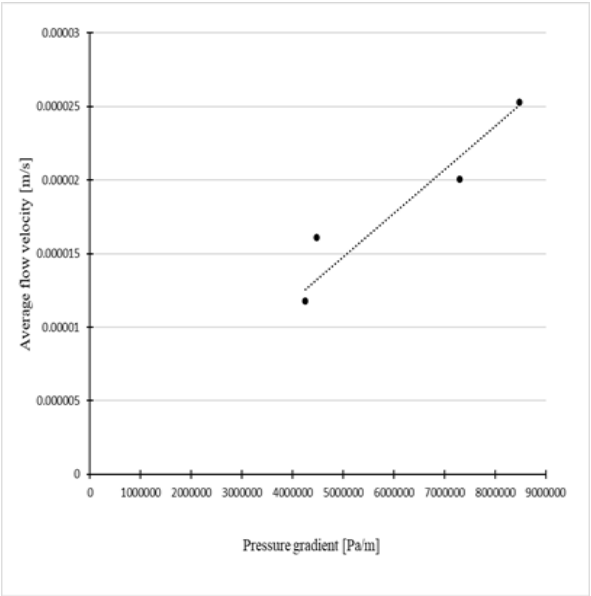

a – 200-75

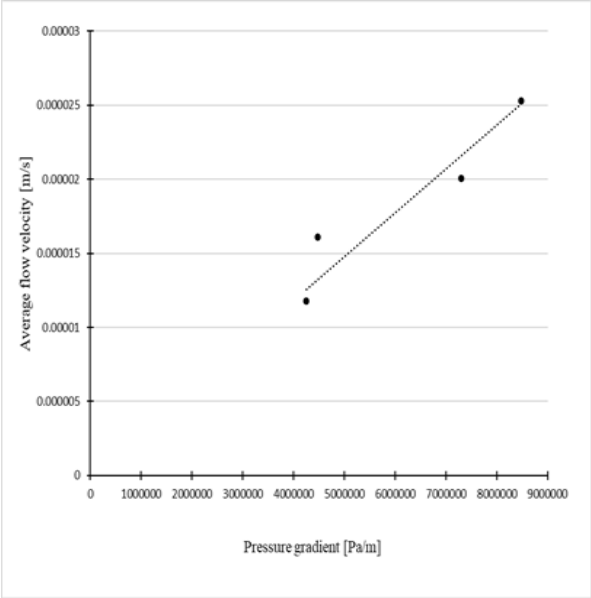

b – 200-85

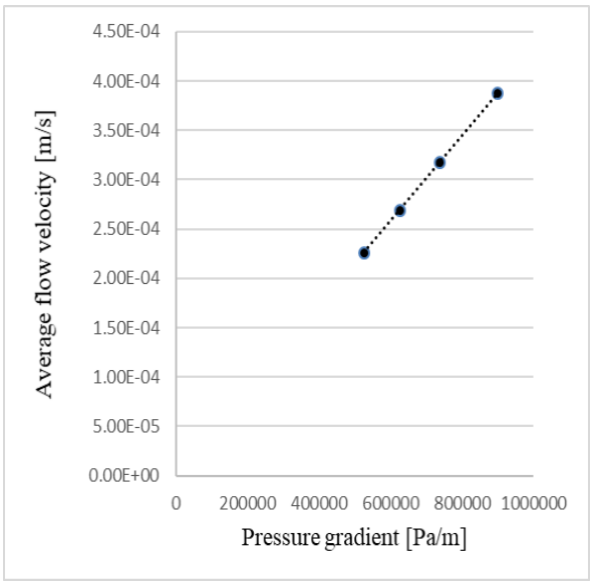

c – 500-75

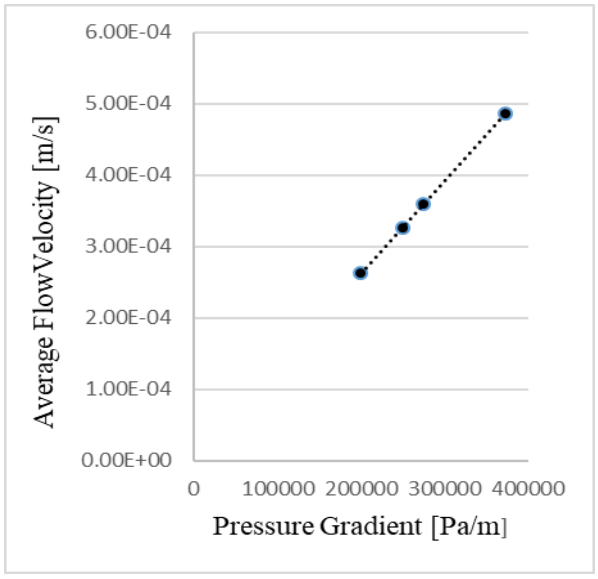

d – 500-85

Fig. 12 - Relationship between the average flow velocity and pressure gradient, a: 200-75, b: 200-85, c: 500-75, d: 500-85

	Viscosity(Pa·s)	Slope	Permeability (m²)
200-75	79.74	$9.70032 \cdot 10^{9}$	$8.22035 \cdot 10^{-9}$
200-85		$4.00581 \cdot 10^{9}$	$1.99061 \cdot 10^{-8}$
500-75		$2.31325 \cdot 10^{9}$	$3.44710 \cdot 10^{-8}$
500-85		$7.66463 \cdot 10^{8}$	$1.04036 \cdot 10^{-7}$

Fig. 13 Table of values used to calculate permeability

The results of the CFD simulations show a similar relationship between fiber diameter and porosity with the permeability of the porous medium. Just as with the experimental results, it is evident that the samples with 85% porosity were more permeable than those of 75% porosity, and the samples of 500µm diameter were more permeable than those of 200µm diameter.

The permeability values obtained in the simulations was higher in comparison to both experimental methods. This could be due to the difference in structure and orientation of the fibers. The uniformity of the fiber spacing could offer less resistance in the flow, and allow the flow velocity to increase, in turn increasing the permeability. This could suggest a relationship between the pore size and shape with permeability.

Applications

Combining the results of both experimental methods and the simulations, there are quite a few applications plausible for the different porous media.

Porous media are ideal for applications as filters. The results in this study, and similar studies of porous materials, suggest that media of less porosity are better for filters Low porosity materials slow flow

velocity, make it easier to catch impurities you want filtered, more accurate than those of high porosity. This idea is also supported in the findings of the study by Fu et al, which focuses on flow and heat transfer characteristics specifically in engine particulate filters. The study found similarly that the ordered structured material's permeability was higher than that of the disordered structured material's permeability, but the filtration deficiency was lower [12]. The study by Wang et al on oil-water separation in porous metals suggests that porous media would be useful filtration devices couples with coatings or membranes to enhance the filtration capabilities [3]. The geometry of the metals coupled with the chemical characteristics of a given coating would allow the metal to filter a wide range of particulates in a wide range of liquids and mixtures. While the study by Anderson et al on filters used in dairy wastewater used PVC and sintered glass, the results further support that low porosity media are better for filtration applications than those of high porosity [2]. Coupled with the concepts from the Fu et al study, porous metal media with coatings could prove to be more cost effective filters in wastewater filtration.

The porous media could also be used in thermal applications. A study by Gauna et al on heat transfer in porous metals for cooling applications found that, again, permeability increased with porosity and pore size. The study also showed that increasing the flow rate and decreasing porosity increased the heat transfer performance, suggesting that higher permeability metals may be more ideal for thermal applications [13]. Aluminum itself is an excellent thermal conductor, and coupled with the enhanced heat transfer brought by physical structure of porous materials, would serve well in both heating and cooling apparatus. The study by Atakan et al suggests that highly conductive metals coupled with a complimentary coating can improve the heat transfer and longevity of the metal itself in thermal applications [14]. Especially in adsorptive coatings, the durability of the metal and the coating can save overall time and maintenance.

Applications with fuel cells and solar energy are also fitting for porous metals. Fuels cells themselves are regarded as very important in energy technology for their low environmental impact and ability effectively change chemical fuels to electricity. In order for porous metals to be effective in fuel cell technology, they must be durable to also increase fuel cell duration [15]. Yuan et al suggests that porous metals would be useful as diffusers in polymer electrolyte membrane fuel cell (PEMFC) applications, making the metals in this study good candidates. Rashidi et al reference many studies on the use of porous materials in solar heaters and heat exchangers [16]. It was found in one study that porous heaters always had increased and more effective thermal efficiency. Coupled with the thermal efficiency of aluminum, the media in this study could fitting in solar energy applications.

The samples in this study could also be suitable for sound absorption applications. The high stiffness and heat capacity of aluminum, the physical structure of the porous medium that is known to enhance heat transfer, and light weight are ideal for noise control in high pressure applications [17]. The sound absorption performance increases with the sound pressure level, and the flow velocity increases with sound pressure, indicating the more porous metals would be better for applications of this nature. Porous glass wool fibers are the most used material in sound adsorption. Despite its wide use and low cost, it is not the most optimal material for this application. Glass wool fibers have low tolerance to thermal changes, low stiffness, low strength, and the efficiency of absorptivity declines with time [18]. Aluminum has high tolerance to thermal change, high stiffness, high strength, and a longer working life. The stiffness of aluminum and pore size is also directly related to sounds adsorption of metals. The larger the pores and stiffness, the higher the sound adsorption.

Electronic applications such as those in supercapacitors and batteries work well with porous metals. Huang et al [5] discusses the use of porous aluminum oxide as a sensor. This application allows for the monitoring of moisture levels. While the media in this study are not on the nanoscale as the ones in the Huang et al study, it is suggested that the metals in this study, if treated, could be used in larger scale sensing applications.

The applications discussed above were based on the estimates on heat transfer coefficients and flow behaviors from the permeability values calculated in this study. It should be noted, however, that the functionality and suitability of the samples in this study could change for different applications as more information is gathered on the thermal and flow behaviors of the different samples.

Conclusion

This study explored the permeability and its effects on flow properties of the porous fibrous sintered aluminum metals of varying fiber diameter and porosity created by Mitsubishi Materials. It was found that there was a linear relationship between the average flow velocity and pressure gradient for each of the samples studied. As porosity increased, the permeability decreased. These findings provided a foundation for estimates on the currently unknown flow characteristics. In turn, estimations on wide range of applications fitting the material, including, but not limited to, filtration, thermal transport, and energy transport, were possible. The results also suggest that the heat transfer coefficients would increase as permeability increases, which could be further tested in future studies.

References

1 Barari, F., Luna, E., Goodall, R., & Woolley, R. Metal foam regenerators; heat transfer and storage in porous metals. Journal of Materials Research, 2013. 28(17), 2474-2482

2 Anderson, G.K., Kasapgil, B., & Ince, O. Comparison of porous and non-porous media in upflow anaerobic filters when treating dairy wastewater. Water Research (Oxford) (United Kingdom). 1994. Vol: 28, Issue: 7, Page: 1619-1624

3 Wang, H., Hu, X., Ke, Z., Du, C. Z., Zheng, L., Wang, C., & Yuan, Z. Review: Porous Metal Filters and Membranes for Oil-Water Separation. Nanoscale research letters. 2018. 13(1), 284

4 P.S. Liu; G.F. Chen. Porous Materials. Applications of Porous Materials. Tsinghua University Press Limited. Chapter Eight: Applications of Polymer Foams. Pages 383-410

5 Huang, A., He, Y., Zhou, Y. Mater Sci: A review of recent applications of porous metals and metal oxide in energy storage, sensing and catalysis**.** 2019. 54: 949

6 Bahrami, M. Forced Convection Heat Transfer. Notes. Simon Fraiser University. 2015. ENSC 388 (F09)

7 Baloyo, J M. Open-cell porous metals for thermal management applications: fluid flow and heat transfer,Materials Science and Technology. 2017. 33:3, 265-276

8 Huang X., Wang Q., Zhou W., Deng D., Zhao Y., Wen D, Li J. Morphology and transport properties of fibrous porous media. Powder Technology. 2015. 283, 618–626

9 Jain, A. K., Basu, S. Flow Past a Porous Permeable Sphere: Hydrodynamics and Heat-Transfer Studies. *Ind. Eng. Chem. Res.*2012. 51, 4, 2170-2178

10 Tasaka, R.,

11 Cham. Everyone Can Enjoy CFD! ３次元熱流体解析ソフトウェア 「PHOENICS」. 2019. Website. phoenics.co.jp

12 Fu J., Zhang T., Li M., Li S., Zhong X., Liu X. Study on Flow and Heat Transfer Characteristics of Porous Media in Engine Particulate Filters Based on Lattice Boltzmann Method. Energies. 2019. 12, 3319; DOI 10.3390/en12173319

13 Gauna E., Zhao Y. Numerical Simulation of Heat Transfer in Porous Metals for Cooling Applications. Topical Collection: Physical and Numerical Simulations of Materials Processing. Metallurgical and Materials Transactions B. 2017. Volume 48B, 1925

14 Atakan A., Fueldner G., Munz G., Henninger S., Tatlier M. Adsorption kinetics and isotherms of zeolite coatings directly crystallized on fibrous plates for heat pump applications. Applied Thermal Engineering. 2013. 58, 2013, 273-280

15 Yuan W., Tang Y., Yang X., Wan Z. Porous metal materials for polymer electrolyte membrane fuel cells – A review. Applied Energy. 2012. 94, 2012, 309-329

16 Rashidi S., Esfahani J., Rashidi A. A review on the applications of porous materials in solar energy systems. Renewable and Sustainable Energy Reviews. 2017. 73, 2017, 1198-1210

17 Wang X., Li Y., Chen T., Ying Z. Research on the sound absorption characteristics of porous metal materials at high sound pressure levels. Advances in Mechanical Engineering. 2015. Vol 7(5), 1–7

18 Liu P.S., Chen G. F. Chapter Three - Application of Porous Metals. Porous Materials. Processing and Applications. 2014. 113-188